Because scipting is unsupported or disabled on your browser, please click the button below...

View Fulltext

Appl. Phys. A 73, 723–730 (2001) / Digital Object Identifier (DOI) 10.1007/s003390100968

Applied Physics A
Materials
Science & Processing

Orbital correlations in doped manganites

J.P. Hill[1,*], C.S. Nelson[1], M. v. Zimmermann[1], Y.-J. Kim[1], D. Gibbs[1], D. Casa[2], B. Keimer[3], Y. Murakami[4], C. Venkataraman[5], T. Gog[5], Y. Tomioka[6], Y. Tokura[6,7], V. Kiryukhin[8], T.Y. Koo[8], S.-W. Cheong[8,9]

[1] Department of Physics, Brookhaven National Laboratory Upton, N.Y. 11973-5000, USA
[2] Department of Physics, Princeton University Princeton, N.J. 08544, USA
[3] Max-Planck-Institut für Festkörperforschung, 70569 Stuttgart, Germany
[4] Photon Factory, Institute of Materials Structure Science High Energy Accelerator Research Organization, Tsukuba 305-0801, Japan
[5] CMC-CAT, Advanced Photon Source, Argonne National Laboratory Argonne, Ill. 60439, USA
[6] Joint Research Center for Atom Technology (JRCAT) Tsukuba 305-0033, Japan
[7] Department of Applied Physics, University of Tokyo, Tokyo 113-0033, Japan
[8] Department of Physics and Astronomy, Rutgers University, Piscataway, N.J. 08854, USA
[9] Bell Laboratories, Lucent Technologies, Murray Hill, N.J. 07974, USA

Received: 22 May 2001/Accepted: 4 July 2001/Published online: 5 October 2001 –

Abstract. We review our recent X-ray scattering studies of charge and orbital order in doped manganites, with specific emphasis on the role of orbital correlations in $Pr_{1-x}Ca_xMnO_3$. For $x = 0.25$, we find an orbital structure indistinguishable from the undoped structure and long-range orbital order at low temperatures. For dopings $0.3 \leq x \leq 0.5$, we find scattering consistent with a charge and orbitally ordered CE-type structure. While in each case the charge order peaks are resolution limited, the orbital order exhibits only short-range correlations. We report the doping dependence of the correlation length and discuss the connection between the orbital correlations and the finite magnetic correlation length observed on the Mn^{3+} sublattice with neutron-scattering techniques. The physical origin of these domains, which appear to be isotropic, remains unclear. We find that weak orbital correlations persist well above the phase transition, with a correlation length of 1–2 lattice constants at high temperatures. Significantly, we observe similar correlations at high temperatures in $La_{0.7}Ca_{0.3}MnO_3$, which does not have an orbitally ordered ground state, and we conclude that such correlations are robust to variations in the relative strength of the electron–phonon coupling.

PACS: 71.28.+d; 71.38.-k; 78.70.Ck

The strongly correlated transition metal oxides are characterized by a wide diversity of ground states, ranging from antiferromagnetic to ferromagnetic and from insulating to superconducting. Further, in many cases transitions between these disparate ground states can be driven by apparently small changes in some parameter, such as the chemical doping or temperature. The origin of this dramatic sensitivity is believed to lie in the fact that no single degree of freedom dominates the response, but rather a number of degrees of freedom may be active. These can include the spin, charge, lattice and orbital degrees of freedom. The ground state is then determined by the interplay between the competing interests of the relevant degrees of freedom. However, despite this qualitative understanding, a complete description of the electronic behavior in transition metal oxides has proved elusive. Elucidating this behavior remains one of the central goals in condensed matter physics today.

The perovskite manganites provide an especially illuminating example of this interplay among the various interactions, since in these materials all the degrees of freedom are active and the balance between them may be conveniently altered (see, e.g., [1]). As a result, much work has been done to understand their magnetic ground states and lattice distortions, dating back to the early work in the 1950s [2, 3]. However, less is known about the roles of charge and orbital order in these materials. The classic work of Goodenough [4] has nevertheless served as a guide to their ordered arrangements, as supplemented, for example, by detailed measurements of the crystal structure and of the temperature dependence of the lattice constants (see [5, 6], for example).

This situation has changed during the last two years, following the detection of orbital and charge order by resonant X-ray scattering techniques [7–32]. Specifically, it has been found that the sensitivity of X-ray scattering to these structures can be significantly enhanced by tuning the incident X-ray energy to the transition metal K-absorption edge. Thus, it appears possible to characterize the orbital and charge ordering on a microscopic scale, and to study their response to temperature changes or to an applied magnetic field. As far as we are aware, resonant X-ray scattering studies of these materials have now been extended to include $La_{0.5}Sr_{1.5}MnO_4$ [7], $LaMnO_3$ [8], $La_{1-x}Sr_xMnO_3$ [12, 14], $Pr_{1-x}Ca_xMnO_3$ [15, 16], V_2O_3 [17], $YTiO_3$ [18], $LaTiO_3$ [19], $LaSr_2Mn_2O_7$ [20], DyB_2C_2 [21, 22], NaV_2O_5 [23], $LaVO_3$ [24], Fe_3O_4 [25], $La_{1-x}Sr_{1+x}MnO_4$ [26], UPd_3 [27], CeB_6 [28] and $Nd_{0.5}Sr_{0.5}MnO_3$ [29, 30], and this list continues to grow.

In this paper, we review our recent X-ray scattering studies of $Pr_{1-x}Ca_xMnO_3$ (PCMO) with $x = 0.25$, 0.3, 0.4 and 0.5. Further, the $x = 0.3$ results are compared with those of $La_{0.7}Ca_{0.3}MnO_3$ (LCMO system). For PCMO, detailed studies have been made of the temperature dependence of the orbital and charge order scattering. For $x = 0.3$, 0.4 and

*Corresponding author. (Fax: +001-631/344-2739, E-mail: hill@bnl.gov)

0.5, below a doping-dependent ordering temperature T_{CO}, the diffraction pattern is found to be consistent with the CE-type charge and orbitally ordered structure. Surprisingly, our studies reveal that long-range orbital order is never established in these samples, although long-range charge order is observed in each case. In contrast, for $x = 0.25$ we observe only long-range orbital order, consistent with the undoped structure and with no indication of any charge ordering. Portions of this work have been published elsewhere [16, 17, 34].

1 Experiment

The PCMO crystals used in the present experiments were grown using floating-zone techniques at JRCAT. (0,1,0) surfaces were cut from cylinders of radius 3 mm and polished with fine emery paper and diamond paste. The mosaic widths of the samples as characterized at the (0,2,0) bulk Bragg reflections (in orthorhombic *Pbnm* notation) were typically $\approx 0.2°$ (FWHM). These values varied by small amounts as the beam was moved across the surface of each crystal, reflecting its mosaic distribution. The growth techniques and basic transport properties of these crystals have been described in detail elsewhere [34–36]. The LCMO sample was grown using floating-zone techniques at Bell Laboratories and had a similar mosaic. It was fully twinned with a (110)/(002) surface normal. For convenience, we adopt the (110) indexing of the surface-normal throughout this paper [33].

The X-ray scattering experiments were carried out at the National Synchrotron Light Source on beamline X22C, and at the Advanced Photon Source, beamline 9IDB, CMC-CAT. X22C is equipped with a bent, toroidal focusing mirror and a Ge(111) double crystal monochromator arranged in a vertical scattering geometry. The optics for 9IDB were comprised of a double-crystal Si(111) monochromator and a flat harmonic rejection mirror. A Ge(111) analyzer crystal was employed in the low-temperature experiments, and a Gr(002) analyzer for the high-temperature work. All data were taken with the incident X-ray energy in the vicinity of the Mn K-edge resonance at $E = 6.555$ eV.

2 Phase behavior of the PCMO system

At room temperature, the crystal structure of PCMO is orthorhombic (*Pbnm*). Characteristic of the perovskite manganites, each Mn atom lies at the center of the octahedron defined by the oxygen atoms at the corners. Single layers of Pr atoms lie between the layers of octahedra. A schematic phase diagram for PCMO versus Ca concentration and temperature [5, 35] is shown in Fig. 1. For small x ($0.15 \leq x \leq 0.3$) and at low temperatures, PCMO is a ferromagnetic insulator and is believed to exhibit an in plane $(a-b)$ orbitally ordered ground state analogous to that observed in $LaMnO_3$. The electronic configuration of the $Mn^{3+}(d^4)$ ions is (t_{2g}^3, e_{g^1}) with the t_{2g} electrons localized at the Mn sites. The e_g electrons are hybridized with the oxygen $2p$ orbitals and are believed to participate in a cooperative Jahn–Teller distortion of the MnO_6 octahedra [5]. This leads to a $(3x^2 - r^2)$–$(3y^2 - r^2)$-type of orbital order of the e_g electrons in the $a-b$ plane with the oxygens displaced along the direction of extension of the e_g orbitals.

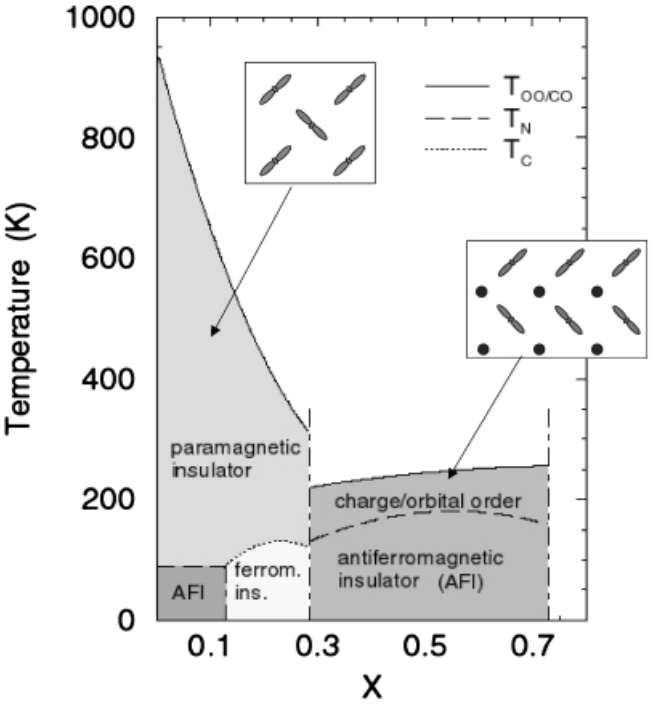

Fig. 1. Composition–temperature phase diagram of $Pr_{1-x}Ca_xMnO_3$ (PCMO) in zero magnetic field (following [5]). The *solid lines* indicate the charge/orbital transition temperature ($T_{OO/CO}$); antiferromagnetic transitions (T_N) are marked with *dashed lines* and ferromagnetic transitions (T_C) with *dotted lines*. The two *insets* represent schematics of the in-plane orbital and charge ordered structures. Only Mn ions are represented. The *elongated shapes* represent $3z^2 - r^2$ orbitals on Mn^{3+} sites. The *circles* represent Mn^{4+} sites

A schematic of this orbitally ordered state for $x = 0.25$ is shown in Fig. 1. The excess Mn^{4+} ions in this material are believed to be disordered; however, recently other proposals have been put forward [37–40]. To date, however, we have found no evidence of such ordering. The orbital period is twice that of the fundamental Mn spacing, so that orbital scattering appears at structurally forbidden reflections. In orthorhombic notation, for which the fundamental Bragg peaks occur at (0,2k,0), the orbital scattering then occurs at (0,k,0).

For Ca concentrations $0.3 \leq x \leq 0.7$, PCMO becomes an antiferromagnetic insulator at low temperatures and exhibits colossal magnetoresistance in applied magnetic fields, with the metal–insulator transition occurring between 5 and 8 T [35]. The insulating phase is accompanied by charge ordering among the Mn^{3+} and Mn^{4+} ions, and orbital ordering of the e_g electrons on the Mn^{3+} sites. The large conductivity results from a delocalization of these e_g electrons and the destruction of the charge and orbital order. The fraction of Mn ions in the Mn^{4+} state is determined largely by the concentration of Ca ions. Thus, by varying the Ca concentration, it is possible to move from a ground state with orbital order and no charge order to one in which both charge and orbital order are observed. The proposed ground state [5] for the $0.3 \leq x \leq 0.7$ concentrations is shown in Fig. 1. Note that the same structure was proposed for this entire region [5]. Clearly, for $x \neq 0.5$, this picture cannot be strictly correct. Jirak et al. [5] proposed that the extra electrons present for $x \leq 0.5$ could be accommodated in such a structure by a partial occupancy of the $3z^2 - r^2$ orbitals of the nominal Mn^{4+} sites. Other possibili-

ties include small Mn^{3+}-rich regions, higher-order structures, or small regions of orbital disorder. As discussed below, our data reveal that, in fact, the orbital order is not long-range in these compounds, although the charge order is. In the orthorhombic notation, the charge-order reflections occur at $(0,2k+1,0)$ and the orbital order reflections at $(0,k+1/2,0)$. Note that the orbital period ($=2b$) in the $x=0.4$ and 0.5 compounds differs from that occurring in samples with $x<0.3$ ($=b$), as a result of the presence of charge ordering.

The magnetic structure of these compounds at low doping ($0.15 \le x \le 0.3$) is ferromagnetic with $T_C \approx 140$ K. Compounds with higher doping ($0.3 \le x \le 0.75$) are CE-type antiferromagnets with $T_N = 170$ K for x between 0.4 and 0.5 [5].

3 Low-temperature correlations

High-resolution longitudinal scans through the Bragg, charge and orbital ordering peaks of the $x=0.4$ and 0.5 samples are superimposed on each other for comparison in Fig. 2 a,b. These data were obtained at low temperatures (10 K) in the ordered phase using a Ge(111) analyzer. Solid lines indicate the results of scans through the (0,2,0) Bragg peaks; open circles indicate scans through (0,2.5,0) orbital peaks; and filled circles give the results obtained for the (0,3,0) and (0,1,0) reflections of the charge ordered peaks of the $x=0.4$ and 0.5 samples, respectively. It is clear from the figure that the Bragg and charge ordered peaks have similar widths, approximately corresponding to the momentum-transfer resolution at each Q. This implies that the correlation lengths of the structure and of the charge order are each at least 2000 Å for both the $x=0.4$ and the $x=0.5$ samples. The small differences in width between the structural and charge order peaks probably reflect the Q-dependence of the resolution function. In contrast, the orbital ordering peaks in both samples are significantly broader than the resolution, implying much smaller orbital domain sizes. We find similar behavior in $x=0.3$ samples.

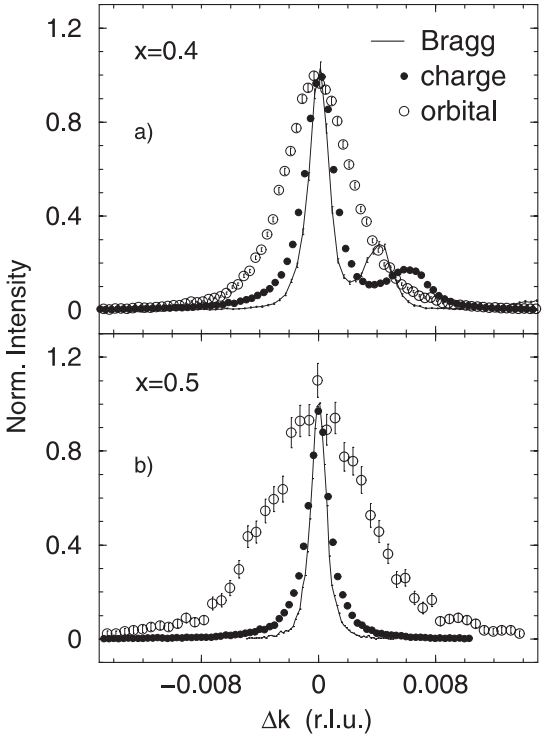

Fig. 2. a Longitudinal scans of the Bragg (0,2,0), the charge (0,1,0), and the orbital (0,2.5,0) reflections of the $x=0.4$ sample at $T=8$ K. The secondary peaks to the right of the charge order and Bragg reflections arise from structural twins. **b** The same for the $x=0.5$ sample. Data have been normalized to the same peak intensity to facilitate comparison

In order to extract longitudinal correlation lengths for the orbital order peaks, we fit these data to a Lorentzian-squared lineshape, convolved with a Lorentzian-squared resolution function – the latter being determined by fits to the (0,2,0) structural Bragg peak. This lineshape was chosen based simply on the quality of the fit, there is no theoretical justification for it. However, without an analytical form for the correlation function, we are forced to choose a definition for the correlation length, ξ. We take the simplest choice, $\xi = 1/\Delta k$, where Δk is the HWHM of the Lorentzian-squared. This definition is somewhat generic – given a particular form for the correlation function, and thus an appropriate lineshape, the actual correlation length of that model may differ slightly from those quoted here. However, it is unlikely to significantly change the results, and in the absence of such a description, we believe that this definition provides a reasonable empirical characterization of the orbital domain state.

At low temperatures, we find $\xi(x=0.3$, sample I, the "disk" sample$) = 60\pm10$ Å, $\xi(x=0.3$, sample II, the "tombstone" sample$) = 170\pm20$ Å, $\xi(x=0.4) = 320\pm10$ Å and $\xi(x=0.5) = 160\pm10$ Å. (Note, the two $x=0.3$ samples had similar mosaics and the same reflections were studied. The origin of the differences in the orbital correlations lengths is not clear.) It is important to emphasize that the associated charge order of the CE charge and orbitally ordered state does exhibit significantly longer-range correlations ($\ge$2000 Å) in each case. Thus these results indicate that for these samples an orbital glass-like state exists on a well-ordered lattice of charge order. In regard to the concentration dependence of these results, in an earlier publication [14] we noted that $\xi(x=0.5) \le \xi(x=0.4)$, despite the fact that the $x=0.4$ sample did not have "enough" Mn^{4+} sites to form the ideal structure. We then speculated that the shorter correlation length in the $x=0.5$ structure resulted from the fact that this sample was closer to tetragonality and that therefore domain walls which switched a and b axes were more likely. However, the new $x=0.3$ results do not follow the trend of longer orbital correlation lengths for more tetragonal samples. This suggests some other mechanism is controlling the correlation length. We return to this point below.

The discovery of an orbital domain state sheds light on recent neutron-diffraction studies of $Pr_{0.5}Ca_{0.5}MnO_3$ [41, 42], and powdered $La_{0.5}Ca_{0.5}MnO_3$ [6]. In the PCMO ($x=0.5$) it was shown that the magnetic correlation length was finite. In $La_{0.5}Ca_{0.5}MnO_3$, which also exhibits the CE-type magnetic structure with orbital and charge order [6], separate magnetic correlation lengths were extracted for the Mn^{3+} and Mn^{4+} magnetic sublattices, with the remarkable result that they were quite different: $\xi_{3+}^{mag} = 250-450$ Å and $\xi_{4+}^{mag} \ge 2000$ Å, respectively. The authors proposed antiphase domain walls composed of "mis-oriented" e_g orbitals to explain the magnetic disorder of the Mn^{3+} sublattice. Randomly spaced, domain walls of this type would break the orbital coherence but preserve the charge order coherence (Fig. 3).

Further, as realized in [6], these domain walls affect the magnetic correlations on the Mn^{3+} and Mn^{4+} sublattice differently. This is illustrated in Fig. 3, in which the signs at each site denote the spin direction at that site. The ideal CE-type charge and orbitally ordered antiferromagnetic structure is shown in Fig. 3a, together with various possible domain walls (Fig. 3b–e). Figure 3b corresponds to the domain wall proposed in [6] with an orbital phase shift running perpendicular to the orbital propagation vector. Inspection of Fig. 3b reveals that the magnetic coherence on the Mn^{3+} sublattice is broken by this domain wall, while the Mn^{4+} sublattice remains unaffected. Such orbital domain walls would therefore explain the observed magnetic neutron-diffraction data. Our observation of orbital correlation lengths of similar values to the Mn^{3+} magnetic correlations strongly suggests that Radaelli et al. [6] were correct in their speculation and that we have observed these antiphase domains directly in PCMO. Note that these domains are believed to be static and do not correspond to the (dynamic) orbital fluctuations inferred from magnetic neutron-diffraction investigations of the ferromagnetic spin fluctuations in PCMO, which disappear below T_N [41].

If all of the domain walls were of the type shown in Fig. 3b, however, then the orbital coherency would only be broken in one direction and very anisotropic domains would be observed. To look for such anisotropy, we measured the correlation lengths in the other two directions, i.e. perpendicular to $\boldsymbol{b}^*$, the orbital propagation direction. These meas-

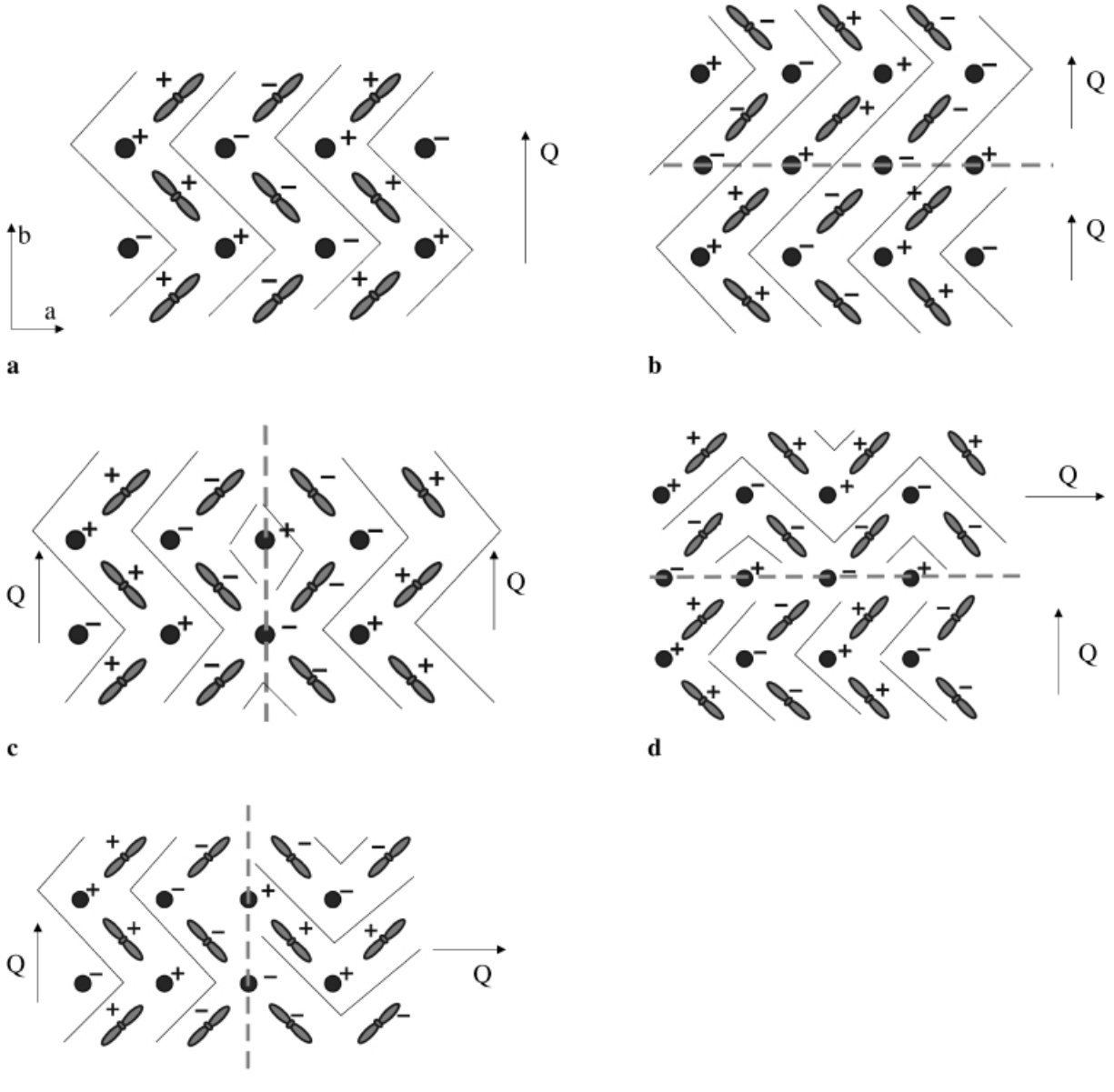

Fig. 3. a–e Schematic of the CE-type charge and orbitally ordered antiferromagnetic state and possible domain walls. Signs indicate spin components at each Mn site. **a** Ideal structure. **b–e** Various domain walls which preserve the charge order but not the orbital coherence. Domain walls in **b** and **c** preserve the orbital propagation vector (0,0.5,0), and those in **d** and **e** rotate it by 90 °. Note that in each case the magnetic coherence of the Mn^{3+} sublattice has been broken, relative to **a**, but not that of the Mn^{4+} sublattice. The *solid lines* outline ferromagnetic stripes in these structures. In each case, the *b* crystallographic axis runs vertically, the *a* axis horizontally

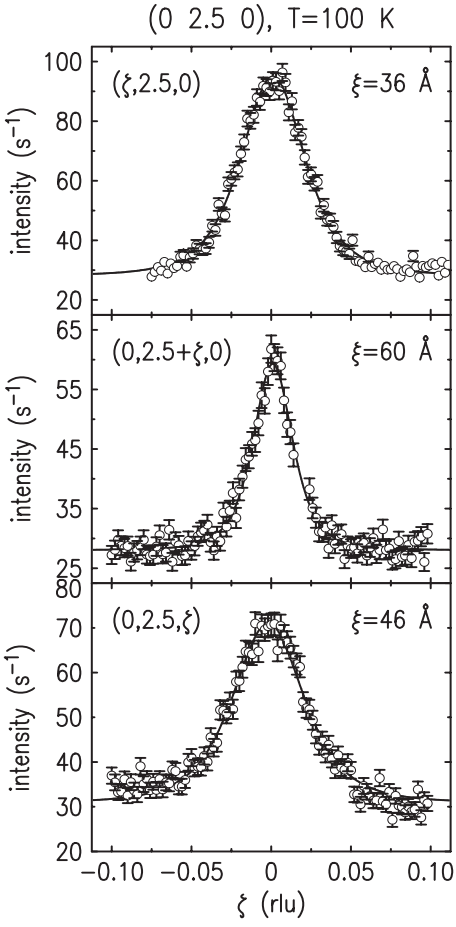

Fig. 4. Scans through the (0,2.5,0) orbital reflection in $Pr_{0.7}Ca_{0.3}MnO_3$, sample I, along each of the three orthorhombic axes in reciprocal space. The correlation lengths quoted in the panel were extracted from fits to the data, as discussed in the text

urements were carried out on the $x = 0.3$ sample I, the "disk" sample, with a Ge(111) analyzer and are shown in Fig. 4. We find that the orbital domains in this sample are approximately isotropic, with slightly reduced correlation lengths in the two transverse directions, of $\xi_H = 36$ Å and $\xi_L = 46$ Å along the H and L directions respectively. (Note that these two correlation lengths correspond to widths significantly broader than the resolutions in these two directions, which are determined by the sample mosaic and the out-of-plane collimation, respectively. Thus no correction for resolution effects was made.) These results indicate the presence of domain walls, other than those of Fig. 3b, that run in other directions and which disrupt only the orbital correlations.

Before discussing this further, we point out that it appears that this orbital glass-like state is common in manganites with the CE-type charge and orbital structure – we have observed it in all PCMO samples studied; the $La_{0.5}Ca_{0.5}MnO_3$ neutron-diffraction data indicate that it is also present in this compound [6], and very recent X-ray work on $(La_yPr_{1-y})_{1-x}Ca_xMnO_3$ revealed the presence of a similar orbital glass/charge ordered state in that system as well [42]. Finally, in $La_{0.67}Ca_{0.33}MnO_3$ an incommensurate state is observed. The incommensurability is believed to be the result of an ordered array of domain walls (discommensurations) breaking the coherence of an otherwise commensurate CE-type structure. The spacing of these domain walls can be obtained from the incommensurability and is 200 Å.

In each of these cases, orbital domain walls spaced by a few hundred Angstroms are observed in an ordered array of Mn^{3+} and Mn^{4+} sites. It is interesting to consider the underlying energetics that might determine this length scale. There are a number of different contributions to the cohesive energy of the CE state shown in Fig. 3a (in the third dimension, an identical charge and orbitally ordered layer is stacked on top of the one shown in Fig. 3a, with all the spins reversed) [4, 44, 45]. The first of these is the magnetic bonds, both ferromagnetic and antiferromagnetic, resulting from the presence or absence of occupied orbitals between the various Mn sites, and mediated by the oxygens [4]. In the antiferromagnetic state shown in Fig. 3a, all these are satisfied, that is, none of the bonds are frustrated. A second contribution is the Coulomb energy of the Mn charges. This is minimized by the in-plane charge ordered lattice shown. Third, the CE structure contains a series of ferromagnetic zig-zag stripes oppositely aligned and running through the $a-b$ plane (Fig. 3a). The e_g electrons are free to hop along these zig-zags as in the case of a double-exchange-like ferromagnet. This allows them to increase their kinetic energy in this antiferromagnetic insulating state. Finally there is the electronic energy gain associated with the local Jahn–Teller distortion around each Mn^{3+} which removes the degeneracy of the $3z^2 - r^2$ and $x^2 - y^2$ orbitals (so-called "non-cooperative phonons" [44]) and the gain in energy associated with the orbital coherency which results from the fact that neighboring Mn sites share oxygens ("cooperative phonons" [44]). These last two come at the expense of lattice energy resulting from the associated oxygen motion.

In Fig. 3b–e, we compare possible domain walls in the $a-b$ plane that break the orbital order coherence, but preserve the charge order coherence. The first thing to note is that in each case all the magnetic bonds are satisfied, that is, there is no magnetic frustration introduced by these domain walls. Secondly, in each case, the magnetic coherence of the Mn^{4+} lattice is left undisturbed, while that on the Mn^{3+} is broken. In the first two (Fig. 3 b,c) the orbital coherence is broken along the b and a directions respectively, but in each case the propagation vector is left unchanged – along b. In the second two cases (Fig. 3 d,e) the orbital correlations are again broken along the b and a directions, respectively. However, in these cases, the propagation vector is rotated by 90° across the domain wall.

In light of the energy considerations discussed above, we see that the domain walls of the type shown in Fig. 3b cost very little energy. They do not break any magnetic bonds, and preserve the ferromagnetic zig-zag stripes, simply adding an extra straight section to one of the "zigs" (though there is an energy cost, relative to the ground state, associated with straight lines of 1D ferromagnetism [44]). The charge order coherence is not disturbed, so there is no Coulomb price to pay relative to the ground state and there are the same number of local distortions as there are in the ideal structure. The principal cost, then, relative to the ideal structure is due to the fact that along the domain wall the oxygen motions are not cooperative. Similar arguments can be made about the domain walls shown in Fig. 3c. For Fig. 3 d,e, the argument is slightly different, since in each case, in addition to the energy cost of the domain wall itself, there is also some energy cost associated with the part of the sample that has the "wrong"

orientation of the propagation vector, i.e. along a local a axis. For PCMO, $x = 0.5$, however, the difference between a and b is very small [42], and thus the energy cost might also be expected to be small.

If the orbital twins shown in Fig. 3 d,e coincide with structural twins – that is the a and b crystallographic axes are also interchanged across these walls – then we can rule out these domain walls as limiting the orbital correlations. This is because the structural coherence, as measured at the (0,2,0) reflection, would also be limited by such domain walls, and yet, as we have seen, it exhibits significantly longer correlations than those of the orbital peaks (Fig. 2). However, if such orbital twins exist in a single crystallographic domain, then they would have the desired properties of limiting the orbital coherence, but leaving the charge order and structural coherence unchanged.

The experimental signature of such orbital twins would be a (0.5,0,0)-type orbital peak in a single crystallographic domain sample. In a crystallographically twinned sample, it would be difficult to distinguish such peaks from a (0,0.5,0)-type peak associated with an a axis crystallographic twin. However, in PCMO $x = 0.3$ (the "tombstone" sample), we were able to clearly resolve the (2,0,0) and (0,2,0) reflections, along the nominal (0,k,0) direction, from a and b twins. In this sample, in addition to the (0,0.5,0)-type peaks associated with the b-axis twin, we also observed (0.5,0,0)-type peaks associated with the a-axis twin. Such peaks are consistent with the presence of orbital domains of the type shown in Fig. 3d,e in a single crystallographic domain and are inconsistent with the ideal structure or with orbital domain walls of the type shown in Fig. 3b,c, which do not affect the propagation vector.

The question remains, however, what sets the length scale for the domain wall separation? That is, what is the energy gain associated with the insertion of domain walls? One possibility is that there is an impurity potential arising from the presence of Ca ions in the structure. Local fluctuations in the concentration could pin the orbital order on a particular sublattice and introduce domain walls of the type shown in Fig. 3. While such a scenario is hard to rule out, it does not naturally explain the few-hundred-Angstrom domain size observed. In addition, the Pr and Ca ions are extremely similar in size – Pr^{3+} is 1.126 Å and Ca^{2+} is 1.12 Å, so any local strains from dopants are expected to be minimal [46].

A second possibility arises from the fact that with the formation of the CE charge and orbitally ordered state, comes a significant change in the lattice constants, which dramatically increases the orthorhombicity. Thus, if each crystallographic domain were to be a single orbital domain, it would have to accommodate a significant strain associated with the increase in a and b lattice constants. However, if it were to break up into a number of orbital domains with propagation vectors in each of the three directions (i.e. domain walls of type in Fig. 3 d,e, together with a third in the out-of-plane direction), then the strain would be minimized in that volume. It may be that balancing the build-up of strain energy associated with the orbital order with the energy cost of domain walls of this type is what is determining the few-hundred-Angstrom domain size [47]. Testing this hypothesis will require detailed energy calculations for the CE charge and orbitally ordered state, the cost of the domain wall and the build up of the long-range strain. It is hoped that these speculations will prompt such calculations

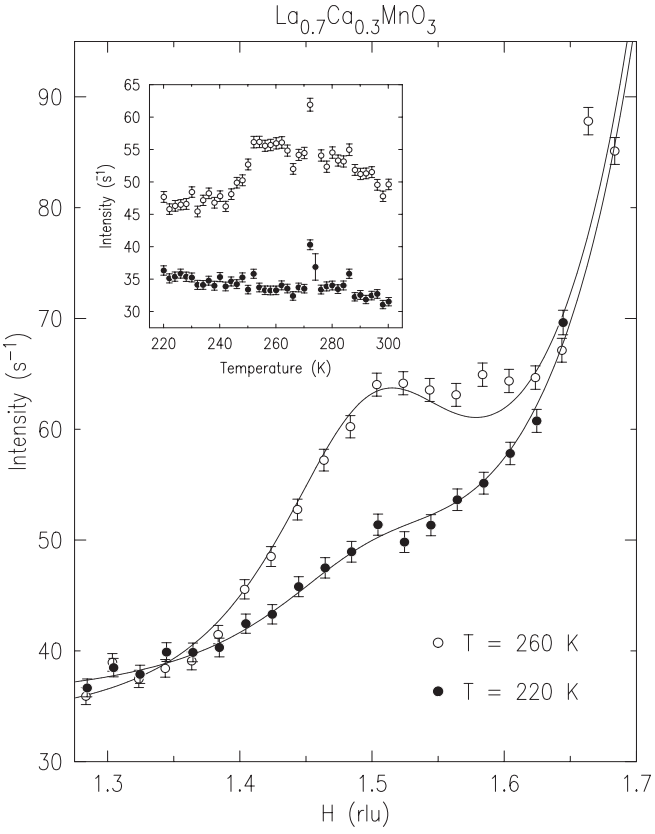

Fig. 5. Reciprocal space scans along H, with Lorentzian-squared fits (*line*), in $La_{0.7}Ca_{0.3}MnO_3$. Data were measured at temperatures of 260 K (*open*) and 220 K (*closed*). The peaks at (1.67,2,0) and (1.5,2.13,0) arise from powder lines and were excluded from the fits. *Inset* shows temperature dependence of scattering intensity at (1.5,2,0) (*open*) and (1.3,2,0) (*closed*). Note that spurious points at temperatures between 270 and 275 K coincided with a beam dump

4 High-temperature correlations

We now turn our attention to a discussion of the high-temperature correlations, i.e. those observed well above the phase transition. We will compare the correlations observed in two manganites that have very different ground states, specifically the PCMO $x = 0.3$ ("tombstone") sample and $La_{0.7}Ca_{0.3}MnO_3$ (LCMO). These are isostructural compounds, both exhibiting *Pbnm* symmetry with the same formal valence on the Mn site. The only difference between the two is the size of the rare-earth ion: La is about 3% bigger than Pr. This has the effect of decreasing the distortion of the Mn–O–Mn bond angles, bringing it closer to the ideal 180° in the LCMO compound, thus increasing the electronic bandwidth and the elastic modulus. Both these effects decrease the relative strength of the electron–phonon coupling [48–50], and as a result, LCMO does not charge and orbitally order, but rather undergoes a transition from an insulating state into a metallic ferromagnetic state below $T_\varrho = 252$ K. By comparing the correlations observed well above the respective phase transitions of these two $x = 0.3$ manganites, we aim to shed light on the role of the relative strength of the electron–phonon coupling.

We begin with the $La_{0.7}Ca_{0.3}MnO_3$ sample. At temperatures above the metal–insulator transition temperature, broad peaks with ordering wavevectors of (0.5 0 0) and (0 0.5 0) and

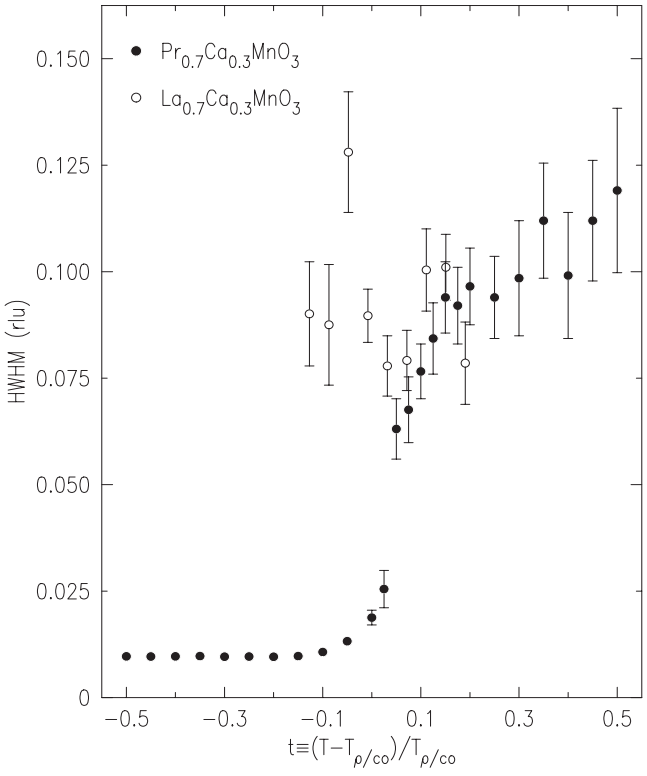

Fig. 6. The fitted HWHM values of the (1.5,2,0) scattering as a function of reduced temperature $\left(t \equiv \frac{T-T_{\varrho/\mathrm{CO}}}{T_{\varrho/\mathrm{CO}}}\right)$, in $La_{0.7}Ca_{0.3}MnO_3$ (*open*) and $Pr_{0.7}Ca_{0.3}MnO_3$ (*closed*)

peak intensities of ~ 20 counts/s (on beamline X22C at the NSLS) were observed. Note that twinning of the sample and the width of the diffuse peaks make it impossible to determine whether or not there is a unique ordering wavevector; however, these wavevectors are consistent with the peaks arising from orbital correlations of the CE-type structure. Representative scans at two temperatures, 260 K and 220 K, are shown in Fig. 5. As the sample was cooled through the transition temperature into the ferromagnetic metallic phase, the peaks abruptly decreased in intensity (see inset to Fig. 5).

Scans were performed along both H and K directions in reciprocal space, and the resulting data fit to Lorentzian-squared lineshapes, as outlined above. The correlation lengths obtained in this manner were found to be temperature independent and approximately isotropic, with a magnitude of 1–2 lattice constants in both directions. The temperature dependence of the fitted values from the H scans are shown in Fig. 6, in which the temperature is recorded as a reduced temperature $t = (T - T_\varrho)/T_\varrho$.

The temperature dependence of the orbital correlations observed in $x = 0.3$ PCMO are also shown in Fig. 6, again as a function of reduced temperature, where in this case T_ϱ is replaced by $T_{\mathrm{CO}} = 200$ K. On warming from below the transition, the HWHM for the PCMO sample is observed to increase rapidly above the transition. However, this broadening does not continue indefinitely, rather the HWHM is observed to saturate around 40 K above T_{CO}. Significantly, the value that it saturates at is the same as that observed in the LCMO, and again corresponds to 1–2 lattice constants.

Thus in these two dissimilar manganites we find very similar high-temperature correlations. Specifically, they have

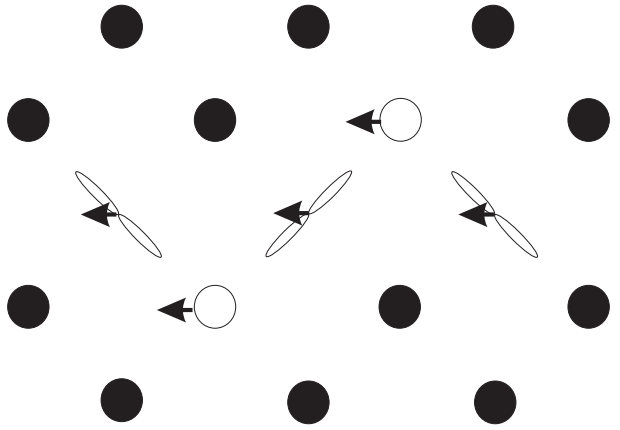

Fig. 7. Schematic of the proposed structure of the observed high-temperature correlations, in the $a-b$ plane. *Open circles* represent Mn^{4+} ions; *elongated figure-of-eights* represent the occupied e_g ($3d_{z^2-r^2}$) orbital of Mn^{3+} ions; *solid circles* represent Mn ions that, on average, have the formal valence and no net orbital order; and *arrows* indicate the in-plane component of the magnetic moment

the same wavevector, size and temperature dependence (at least, far from the phase transition where the intensity in each case increases as the samples are cooled). We suggest that because the same correlations are observed in such different manganite systems, they must be robust to variations in the relative strength of the electron–phonon coupling and are therefore likely to be common to a large class of manganites. This in turn suggests that there may be something fundamental about these correlations that makes them particularly stable. We further speculate that these correlations are in fact small regions of orbital order, as shown in Fig. 7 [33]. A similar picture has been proposed previously [51].

There are a number of pieces of evidence that support this conclusion. First, the wavevector of the scattering is consistent with such a structure (and inconsistent with other possible descriptions, including so-called orbital polarons [38, 39]). Second, these correlations are observed to evolve continuously into the ordered CE structure in the $x = 0.3$ PCMO case. Third, the magnetic interactions within this small piece are all ferromagnetic. Thus, this picture of the orbital correlations is consistent with the neutron-scattering observation of ferromagnetic fluctuations in PCMO above T_{CO} [41]. The fact that they are ferromagnetic also serves to make them particularly robust, since this lessens the energy cost associated with localizing the electrons.

There are a number of possible descriptions that could be applied to these correlations. One could term them bipolarons to emphasize the fact that they represent a pairing of two polaronic distortions around each Mn^{4+} site. An alternative label would be ferromagnetic zig-zags to emphasize the connection with the ordered CE-type structure. Finally, one could refer to them as ferromagnetic clusters – to draw parallels with the phase separation picture of the metal–insulator transition in the manganites. More experiments are required to determine which of these labels, if any, is the more appropriate. For example, investigating the doping dependence, applying a magnetic field or going to yet higher temperatures would shed light on the stability of these correlations against various perturbations and thus help elucidate their nature.

5 Summary

We have used X-ray scattering techniques to study the orbital correlations in a number of doped manganites. In the PCMO series, for $x = 0.25$, we find a ground state with long-range orbital order and no evidence for charge order. For $0.3 \leq x \leq 0.5$, for which the low-temperature ground state is the charge and orbitally ordered CE-type antiferromagnetic structure, the orbital correlations do not develop long-range order, but rather form a domain state. These correlations are approximately isotropic, and domain sizes are on the order of a few hundred Angstroms. In contrast, the charge ordering in this structure does exhibit long-range order. The evidence suggests that orbital domain walls are a common feature of the CE-type manganites; however, there is as yet no theoretical understanding of their origin.

In addition, we have studied the correlations observed at very high temperatures, well above the phase transition. Here, we observe short-range orbital correlations of 1–2 lattice constants in extent. Further, similar correlations are observed in two very different manganites, PCMO ($x = 0.3$) and LCMO ($x = 0.3$), which have antiferromagnetic, charge and orbitally ordered insulating, and ferromagnetic metallic ground states, respectively. We suggest that the presence of similar correlations in such dissimilar manganites demonstrates the robustness of these correlations to changes in the relative strength of the electron–phonon coupling, and we present an intuitively appealing description of these correlations.

Acknowledgements. We acknowledge helpful conversations with S. Ishihara, D.J. Khomskii, S. Maekawa, A.J. Millis, and G.A. Sawatzky. The work at Brookhaven, both in the Physics Department and at the NSLS, was supported by the U.S. Department of Energy, Division of Materials Science, under Contract No. DE-AC02-98CH10886, and at Princeton University by the NSF under Grant No. DMR-9701991. Support from the Ministry of Education, Science and Culture, Japan, by the New Energy and Industrial Technology Development Organization (NEDO), and by the Core Research for Evolution Science and Technology (CREST) is also acknowledged. Work at the CMC beamlines is supported, in part, by the Office of Basic Energy Sciences of the U.S. Department of Energy and by the National Science Foundation, Division of Materials Research. Use of the Advanced Photon Source was supported by the Office of Basic Energy Sciences of the U.S. Department of Energy under Contract No. W-31-109-Eng-38.

References

1. T.A. Kaplan, S.D. Mahanti (Eds.): *Physics of Manganites* (Kluwer Academic, Dordrecht 1999)
2. G.H. Jonker, J.H. Van Stanten: Physica (Utrecht) **16**, 337 (1950); ibid.: **19**, 120 (2000)
3. E. Wollan, W. Koehler: Phys. Rev. **100**, 545 (1955)
4. J. Goodenough: Phys. Rev. **100**, 555 (1955)
5. Z. Jirak, S. Krupica, Z. Simsa, M. Dlouha, S. Vratislav: J. Magn. Magn. Mater. **53**, 153 (1985)
6. P.G. Radaelli, D.E. Cox, M. Marezio, S.-W. Cheong: Phys. Rev. B **55**, 3015 (1997)
7. Y. Murakami, H. Kawada, H. Kawata, M. Tanaka, T. Arima, Y. Moritomo, Y. Tokura: Phys. Rev. Lett. **80**, 1932 (1998)
8. Y. Murakami, J.P. Hill, D. Gibbs, M. Blume, I. Koyama, M. Tanaka, H. Kawata, T. Arima, Y. Tokura, K. Hirota, Y. Endoh : Phys. Rev. Lett. **81**, 582 (1998)
9. S. Ishihara, S. Maekawa: Phys. Rev. Lett. **80**, 3799 (1998)
10. M. Fabrizio, M. Altarelli, M. Benfatto: Phys. Rev. Lett. **80**, 3799 (1998)
11. I.S. Elfimov, V.I. Anisimov, G.A. Sawatsky: Phys. Rev. Lett. **82**, 4264 (1999)
12. Y. Endoh, K. Hirota, S. Ishihara, S. Okamoto, Y. Murakami, A. Nishizawa, T. Fukada H. Kimura, H. Nohiri, K. Kaneoko, S. Maekawa: Phys. Rev. Lett. **82**, 4328 (1999)
13. P. Fulde: J. Phys. Soc. Jpn. **5**, 154 (2000)
14. P. Wochner et al.: unpublished
15. M. v. Zimmermann, J.P. Hill, D. Gibbs, M. Blume, D. Casa, B. Keimer, Y. Murakami, Y. Tomioka, Y. Tokura: Phys. Rev. Lett. **83**, 4872 (1999)
16. M. v. Zimmermann, C.S. Nelson, J.P. Hill, D. Gibbs, M. Blume, D. Casa, B. Keimer, Y. Murakami, C.-C. Kao, C. Venkataraman, T. Gog, Y. Tomioka, Y. Tokura: cond-mat/0007231 Phys. Rev. B (in press)
17. L. Paolosini, C. Vettier, F. de Bergevin, D. Mannix, W. Neubeck, A. Stunault, F. Yakhou, J.M. Honig, P.A. Metcalf: Phys. Rev. Lett. **82**, 4719 (1999)
18. H. Nakao et al.: unpublished
19. B. Keimer, D. Casa, A. Ivanov, J.W. Lynn, M. v. Zimmermann, J.P. Hill, D. Gibbs, Y. Toguchi, Y. Tokura: Phys. Rev. Lett. **85**, 3946 (2000)
20. Y. Wakabayashi, Y. Murakami, I. Koyama, T. Kimura, Y. Tokura, Y. Moritomo, K. Hirota, Y. Endoh: J. Phys. Soc. Jpn. **69**, 2731 (2000)
21. Y. Tanaka, T. Inami, T. Wakamura, H. Yamauchi, H. Onoderon, K. Ohoyama, Y. Yamaguchi: J. Phys. Condens. Matter **11**, L505 (1999)
22. K. Hirota, N. Oumi, T. Matsumura, H. Nakao, Y. Wakabayashi, Y. Murakami, Y. Endoh: Phys. Rev. Lett. **84**, 2706 (2000)
23. H. Nakao, K. Ohwada, N. Takesue, Y. Fujii, M. Isobe, Y. Ueda, M. v. Zimmermann, J.P. Hill, D. Gibbs, J.C. Woicik, I. Koyama, Y. Murakami: Phys. Rev. Lett. **85**, 4349 (2000)
24. M. Noguchi et al.: Phys. Rev. B **62**, R9271 (2000)
25. J. Garcia et al.: Phys. Rev. Lett. **85**, 578 (2000)
26. Y. Wakabayashi, Y. Murakami, Y. Moritomo, I. Koyama, H. Nakao, T. Kiyama, T. Kimura, Y. Tokura, N. Wakabayashi: J. Phys. Soc. Jpn. **70**, 1194 (2001)
27. D.F. McMorrow, K.A. McEwen, U. Steigenberger, H.M. Ronnow, F. Yakhou: Phys. Rev. Lett. **87**, 057201 (2001)
28. H. Nakao, K. Magishi, Y. Wakabayashi, Y. Murakami, K. Koyama, K. Hirota, Y. Endoh, S. Kuni: J. Phys. Soc. Jpn. **70**, 1857 (2001)
29. K. Nakamura, T. Arima, A. Nakazawa, Y. Wakabayashi, Y. Murakami: Phys. Rev. B **60**, 2425 (2000)
30. P. Hatton: Bull. Stefan Univ. **11**, 337 (1999)
31. M. Benfatto, Y. Joly, C.R. Natoli: Phys. Rev. Lett. **83**, 636 (1999)
32. S. Ishihara, S. Maekawa: Phys. Rev. B **58**, 13 442 (1998)
33. C.S. Nelson, M. v. Zimmermann, J.P. Hill, D. Gibbs, V. Kiryukhin, T.Y. Koo, S.-W. Cheong, D. Casa, B. Keimer, Y. Murakami, Y. Tomioka, Y. Tokura, C. Venkataraman, T. Gog: cond-mat/00011502 Phys. Rev. B (in press)
34. Y. Okimoto, Y. Tomioka, Y. Onose, Y. Otsuka, Y. Tokura: Phys. Rev. B **57**, R9377 (1998)
35. Y. Tomioka, A. Asamitsu, H. Kawahara, Y. Moritomo, Y. Tokura: Phys. Rev. B **53**, 1689 (1996)
36. Y. Tokura, Y. Tomioka: J. Magn. Magn. Mater. **200**, 1 (1999)
37. T. Mizokawa, D.I. Khomskii, G.A. Sawatzky: Phys. Rev. B **61**, R3776 (2000)
38. T. Mizokawa, D.I. Khomskii, G.A. Sawatzky: Phys. Rev. B **63**, 024403 (2001)
39. R. Kilian, G. Khaliullin: Phys. Rev. B **60**, 13 458 (1999)
40. T. Hotta, E. Dagotto: cond-mat/9912469
41. R. Kajimoto, T. Kakeshita, Y. Oohara, H. Yoshizawa, Y. Tomioka, Y. Tokura: Phys. Rev. B **58**, R11 837 (1998)
42. Z. Jirak, F. Damay, M. Hervieu, C. Martin, B. Raveau, G. Andre, F. Bouree: Phys. Rev. B. **61**, 1181 (2000)
43. V. Kiryukhin, B.G. Kim, V. Podzorov, S.-W. Cheong, T.Y. Koo, J.P. Hill, I. Moon, Y.H. Jeong: Phys. Rev. B **63**, 24 420 (2000)
44. S. Yunoki, T. Hotta, E. Dagotto: Phys. Rev. Lett. **84**, 3714 (2000)
45. J. v. d. Brink, G. Khaliullin, D. Khomskii: Phys. Rev. Lett. **83**, 5118 (1999)
46. C. Frontera, J.L. Garcia-Munoz, A. Llobet, M. Respand, J.M. Broto, J.S. Lord, A. Planes: Phys. Rev. B **62**, 3381 (2000)
47. A. Millis: private communication
48. A.J. Millis, P.B. Littlewood, B.I. Shraiman: Phys. Rev. Lett. **74**, 5144 (1995)
49. H. Roder, J. Zang, A.R. Bishop: Phys. Rev. Lett. **76**, 1356 (1996)
50. T. Egami: In *Structure and Bonding*, Vol. 98, ed. by J.B. Goodenough (Springer-Verlag, Berlin, Heidelberg) in press
51. K.H. Kim: et al.: Phys. Rev. B **62**, R11 945 (2000)